


Cite this: *New J. Chem.*, 2024, 48, 10074

# Indium-based quantum dots trapped in solid-state matrices: a one-pot synthesis, thermoresponsive properties, and enhanced micropollutant removal†

Nida Ük,<sup>a</sup> Sümeyye Aykut,<sup>b</sup> Hadi Jahangiri,<sup>c</sup> Ilgın Nar<sup>d</sup> and Caner Ünlü<sup>\*ab</sup>

Indium-based quantum dots (QDs), such as copper indium disulfide and zinc copper indium sulfide, have been the center of research for decades due to their low toxicity and unique photophysical properties. In contrast, versatile indium-based materials like  $\text{In}_2\text{S}_3$  and  $\text{ZnIn}_2\text{S}_4$  have been rarely studied in their QD form because of the challenges in their synthesis and used in solid-state material based applications because of their colloidal nature. In this study, a one-pot single-step method to synthesize  $\text{In}_2\text{S}_3$ ,  $\text{ZnIn}_2\text{S}_4$ , and Cu-doped  $\text{ZnIn}_2\text{S}_4$  QDs trapped in insoluble solid-state oleic acid matrices was developed. The QDs in solid-state matrices exhibited bright orange colored fluorescence with controllable emission properties achieved by altering the chemical composition. Among these QDs, the  $\text{ZnIn}_2\text{S}_4$  QDs displayed thermo-responsive properties. As the temperature increased, the fluorescence intensity of  $\text{ZnIn}_2\text{S}_4$  QDs decreased. In addition, all QDs demonstrated high removal efficiency for micropollutants in the aqueous medium, especially against cationic organic dyes. This study represents one of the first attempts at the direct development of QDs trapped in insoluble solid-state matrices. The QDs in solid-state matrices hold promise for applications in thermal sensors and studies related to the micropollutant removal.

Received 15th March 2024,  
Accepted 9th May 2024

DOI: 10.1039/d4nj01219d

rsc.li/njc

## Introduction

Indium-based quantum dots (QDs) have long fascinated researchers due to their intriguing photophysical properties and low toxicity, making them promising candidates for various applications.<sup>1–3</sup> Copper indium disulfide QDs, in particular, have been extensively studied in the literature.<sup>1–3</sup> However, the exploration of alternative indium-based materials in their QD form has been relatively limited, with a particular lack of studies focusing on indium sulfide ( $\text{In}_2\text{S}_3$ ) and zinc indium sulfide ( $\text{ZnIn}_2\text{S}_4$ ) QDs, primarily because of their comparatively weak photophysical properties compared to copper indium disulfide QDs.<sup>4–7</sup>

Like most QDs, indium-based QDs have been synthesized in their colloidal form.<sup>1–7</sup> In addition to their superior photophysical properties, colloidal QDs have a non-porous structure with an extremely small size (4–7 nm for the indium based ones),<sup>1–7</sup> making their utilization impractical for water decontamination studies. This is noteworthy even though indium-based materials have often been employed in water decontamination, particularly in the removal of organic micropollutants from aqueous solutions.<sup>8–12</sup>

Environmental conditions, including factors like temperature, pressure, and humidity, are critical for sustaining life, with temperature being particularly crucial due to its narrow tolerance range.<sup>13,14</sup> Monitoring rapid temperature fluctuations, especially in workplaces like mines, is vital for ensuring safety.<sup>13,14</sup> Thermoresponsive materials, specifically thermoresponsive fluorescent compounds, have gained significant attention for their ability to reversibly change fluorescence intensity or emission wavelength in response to temperature variations, making them invaluable in applications such as temperature sensing, biological sensing, and drug delivery.<sup>15–17</sup> Their sensitivity to temperature changes enables precise tracking in complex settings, including challenging work environments and biological systems.<sup>15–17</sup> Although quantum dots are

<sup>a</sup> Istanbul Technical University, Polymer Science and Technology, Maslak, 34469, Istanbul, Turkey. E-mail: canerunlu@itu.edu.tr

<sup>b</sup> Istanbul Technical University, Faculty of Science and Letters, Department of Chemistry, 34469, Maslak, Istanbul, Turkey

<sup>c</sup> Koç University Surface Science and Technology Center (KUYTAM), Koc University, Sariyer 34450, Istanbul, Turkey

<sup>d</sup> Istanbul Technical University Nanotechnology Research and Application Center (ITUNano), Istanbul, Turkey

† Electronic supplementary information (ESI) available. See DOI: <https://doi.org/10.1039/d4nj01219d>


frequently used as thermosensors,<sup>18–20</sup> their colloidal structure limits their utilization in many applications which requires solid-state thermoresponsive materials.

In this study,  $\text{In}_2\text{S}_3$ ,  $\text{ZnIn}_2\text{S}_4$ , and  $\text{Cu:ZnIn}_2\text{S}_4$  QDs trapped in oleic acid based solid-state matrices were developed using a one-pot single-step synthesis technique. These QDs in the size range of 4 nm to 7 nm were dispersed in a solidified network formed by surfactant molecules which was not soluble in any kind of solvent. QDs in solid-state matrices (SSQDs) emitted orange color fluorescence with considerably high fluorescence quantum yields (up to 31%) and by adjusting the composition, the emission characteristics of these SSQDs could be controlled. Notably, the  $\text{ZnIn}_2\text{S}_4$  SSQDs exhibited a unique thermo-responsive behavior. When subjected to heat, the fluorescence of  $\text{ZnIn}_2\text{S}_4$  SSQDs decreased gradually until 100 °C, and completely quenched at 100 °C. Until 160 °C, the decrease in fluorescence was reversible, allowing the fluorescence of  $\text{ZnIn}_2\text{S}_4$  SSQDs to recover at room temperature. Nevertheless, once the temperature exceeded 160 °C, the fluorescence recovery was no longer observable. In addition, the indium-based SSQDs exhibited great potential in water decontamination from organic micropollutants. All the synthesized SSQDs showed significantly high removal efficiency against cationic organic dyes (methylene blue, methyl violet 2B and rhodamine B). In particular,  $\text{In}_2\text{S}_3$  SSQDs were able to remove anionic dyes (methyl orange and sodium fluorescein) with considerably high removal efficiency.

## Materials and methods

### Chemicals

To synthesize SSQDs, copper(I) iodide ( $\text{CuI}$ , 99.9%, Aldrich), indium(III) acetate ( $\text{In}(\text{C}_2\text{H}_3\text{O}_2)_3$ , 99.9%, Aldrich), zinc stearate ( $\text{C}_{36}\text{H}_{70}\text{O}_4$ , technical grade, Aldrich), thioacetamide ( $\text{CH}_3\text{CSNH}_2$ , >99.0%, Aldrich), oleic acid (OA, 90%, Aldrich), and 1-octadecene ( $\text{CH}_3(\text{CH}_2)_{15}\text{CH}=\text{CH}_2$ , technical grade, 90%, Aldrich) were used without further purification.

### Synthesis of copper doped indium zinc sulfide ( $\text{Cu:ZnIn}_2\text{S}_4$ ) SSQDs

0.0267 g (0.14 mmol) of  $\text{CuI}$ , 0.0409 g (0.14 mmol) of  $\text{In}(\text{CH}_3\text{COO})_3$ , 0.0759 g (0.12 mmol) of  $\text{Zn}-(\text{CH}_3(\text{CH}_2)_{16}\text{COO})_2$ , 0.056 g (0.745 mmol) of thioacetamide, and 0.23 mL (0.72 mmol) of oleic acid were mixed with 1-octadecene (16 mL) in a 250 mL three-necked round reaction flask under a nitrogen atmosphere and heated. As the solution reached nearly 130 °C, all the materials dissolved. The reaction mixture was kept at 150 °C and refluxed for 40 minutes. At the end of 40 minutes, the reaction was stopped by cooling down the reaction mixture. The crude product, SSQDs, precipitated within minutes and was obtained as a solid residue in the reaction medium. Finally, SSQDs were washed with deionized water and acetone and then dried by using dry air at room temperature.

Copper doped indium zinc sulfide SSQDs were also synthesized by using 1-dodecanethiol or 3-mercaptopropionic acid instead of thioacetamide using the same synthesis and purification method.

### Synthesis of zinc indium sulfide ( $\text{ZnIn}_2\text{S}_4$ ) SSQDs

0.0409 g (0.14 mmol) of  $\text{In}(\text{CH}_3\text{COO})_3$ , 0.0759 g (0.12 mmol) of  $\text{Zn}-(\text{CH}_3(\text{CH}_2)_{16}\text{COO})_2$ , 0.056 g (0.745 mmol) of thioacetamide, and 0.23 mL (0.72 mmol) of oleic acid were mixed with 1-octadecene (16 mL) in a 250 mL three-necked round bottom reaction flask under a nitrogen atmosphere and heated. As the solution reached nearly 130 °C, all the materials dissolved. The reaction mixture was kept at 150 °C and refluxed for 40 minutes. At the end of 40 minutes, the reaction was stopped by cooling down the reaction mixture. The crude product, SSQDs, precipitated within minutes and was obtained as a solid residue in the reaction medium. Finally, SSQDs were washed with deionized water and acetone and then dried by using dry air at room temperature.

### Synthesis of indium sulfide ( $\text{In}_2\text{S}_3$ ) SSQDs

In this study, a traditional solvothermal method to synthesize  $\text{Cu:ZnIn}_2\text{S}_4$  colloidal SSQDs was modified by changing the sulfur source to thioacetamide instead of dodecanethiol.<sup>21</sup> 0.0409 g (0.14 mmol) of  $\text{In}(\text{CH}_3\text{COO})_3$ , 0.056 g (0.745 mmol) of thioacetamide, and 0.23 mL (0.72 mmol) of oleic acid were mixed with 1-octadecene (16 mL) in a 250 mL three-necked round reaction flask under a nitrogen atmosphere and heated. As the solution reached nearly 130 °C, all the materials dissolved. The reaction mixture was kept at 150 °C and refluxed for 40 minutes. At the end of 40 minutes, the reaction was stopped by cooling down the reaction mixture. The crude product, SSQDs, precipitated within minutes and was obtained as a solid residue in the reaction medium. Finally, SSQDs were washed with deionized water and acetone and then dried by using dry air at room temperature.

### Observation of the thermoresponsive properties of $\text{ZnIn}_2\text{S}_4$ SSQDs

In order to observe the thermoresponsive properties, approximately 25 mg of  $\text{ZnIn}_2\text{S}_4$  SSQDs were used for the temperature test of the SSQDs. The sample was placed on a black cardboard and heated on a hot plate, increasing the temperature by 10 degrees each time. Once the desired temperature was reached, it was maintained on the hot plate for 4 minutes. Simultaneously, an equivalent amount of the reference sample was subjected to UV light. Images were captured by bringing the heated sample next to the reference. When the temperature surpassed 50 °C, it was observed that the fluorescence color under UV light initially decreased. However, as the observation continued, it was noticed that within approximately 45 seconds, the fluorescence properties returned to its original state. This phenomenon of fluorescence presence upon cooling (at room temperature) and disappearance upon heating persisted up to 160 °C. After reaching 160 °C, it was observed that upon



cooling, the fluorescence properties were lost, indicating structural degradation.

### Treatment of micropollutants with SSQDs

Methylene blue, methyl violet 2B, and rhodamine B were selected as cationic dyes, while methyl orange and sodium fluorescein were chosen as anionic dyes. Aqueous solutions of methyl orange (MO), sodium fluorescein (NF), methylene blue (MB), methyl violet 2B (MV), and rhodamine B (RB) were prepared at a concentration of 20  $\mu\text{M}$ . Subsequently, 1 mL of solutions containing 5 mg of SSQDs were prepared for each micropollutant. The glass vials were subsequently wrapped with aluminum foil and agitated on a shaker at 400 rpm for 24 hours in the absence of light. After 24 hours, a dilution process was performed to better observe the intensity changes in the solutions. 300 microliters of each solution were extracted and diluted to 3 mL with distilled water. The micropollutants were similarly diluted, and measurements were taken using a UV-vis spectrophotometer to observe the differences in absorption intensities.

### Structural and optical characterization of SSQDs

The crystal structures of  $\text{Cu:ZnIn}_2\text{S}_4$ ,  $\text{ZnIn}_2\text{S}_4$ , and  $\text{In}_2\text{S}_3$  SSQDs were analyzed using an RIGAKU SmartLab X-ray diffraction spectrometer with  $\text{Cu K}\alpha$  radiation at a wavelength of 1.5406 Å at 30 kV voltage. The  $\text{Cu:ZnIn}_2\text{S}_4$ ,  $\text{ZnIn}_2\text{S}_4$ ,  $\text{In}_2\text{S}_3$  SSQDs were measured in the 2-theta range between 15° and 70° for 4 seconds with a step size of 0.01°.

The shape and size of the SSQDs were determined using transmission electron microscopy (TEM). TEM measurements were conducted using a JEOL JEM 1220 instrument with an accelerating voltage of 100 kV.

The elemental composition of each nanocrystal was checked by X-ray photoelectron spectroscopy (XPS). XPS measurements were carried out with a Thermo Scientific K-Alpha with a monochromatic 1486.68 eV Al  $\text{K}\alpha$  X-ray line source and a 400  $\mu\text{m}$  beam size.

The surface properties of SSQDs were characterized by attenuated total reflectance FTIR (ATR-FTIR) spectroscopy. The FTIR spectra of the SSQDs were measured in the range of 700–4000  $\text{cm}^{-1}$  by using a PerkinElmer ATR-FTIR spectrophotometer.

The absorption spectrum of SSQDs was recorded using an Agilent double-beam ultraviolet-visible (UV-vis) spectrophotometer. For SSQDs, the QDs were dispersed in dichloromethane and then dropped on quartz glass to form thin films. Afterwards, the absorption spectrum of SSQDs was collected from these thin films.

Fluorescence analysis of SSQDs was performed using a RENISHAW inVia spectrometer with a 532 nm excitation laser, 1% laser power, 10 s acquisition time, and  $\times 50$  objective lens in fluorescence mode at room temperature. The quantum yield (QY) and time resolved fluorescence measurements of SSQDs were conducted with an Edinburgh Instruments FLS1000 spectrometer. For QY measurements of SSQDs, an integrating sphere was used. The time-resolved fluorescence

measurements of SSQDs were performed by using 377 nm excitation wavelength and a  $585 \pm 17$  nm band-pass emission filter.

## Results and discussion

### Trapping QDs in solid-state matrices and formation of SSQDs

To synthesize In-based SSQDs, first, the traditional synthesis method was altered by substituting the surfactant (oleylamine) with another frequently used surfactant for cadmium-based QDs, oleic acid.<sup>22–24</sup> It should be noted that the same procedure to synthesize SSQDs was repeated by keeping oleylamine as the surfactant and colloidal QDs were obtained (see the ESI† for experimental details and Fig. S1 for characterization of the colloidal QDs). As the surfactant was changed, formation of insoluble solid-state materials, in which QDs were dispersed, was observed instead of colloidal QDs. The insoluble nature of solid-state materials arises due to formation of solid networks most likely because of intermolecular interactions between oleic acid molecules, as was observed for different types of QDs<sup>25</sup> and oleic acid alone<sup>26</sup> in the literature before and discussed in more detail later in the text. To determine whether the solid-state material was soluble in any kind of solvent, efforts were made to dissolve the solid-state material in various solvents: toluene, chloroform, acetone, dimethylsulfoxide, *N,N*-dimethylformamide, tetrahydrofuran, methanol, ethanol, and water. However, none of these solvents were successful in dissolving the solid-state material at room temperature, confirming its insoluble nature. In addition, the effect of substituting sulfur precursors from 1-dodecanethiol to thiocetamide was checked by keeping oleylamine as the surfactant when QDs were synthesized in the colloidal form. In the literature, it has been demonstrated that the utilization of various sulfur precursors leads to the formation of distinct crystal structures.<sup>27</sup> Specifically, the use of thioacetamide or 1-dodecanethiol as sulfur precursors has been shown to result in the formation of completely distinct types of crystals.<sup>27</sup> 1-Dodecanethiol has a slow reaction rate and possesses a long carbon chain, which generally leads to the formation of wurtzite type crystals and has been widely used as the S precursor in the synthesis of indium-based quantum dots such as copper indium sulfide and zinc copper indium sulfide.<sup>21,28</sup> On the flip side, thioacetamide exhibits a significantly faster reaction rate, leading to the formation of an entirely distinct crystal type, such as keskerite.<sup>27</sup> It is important to note that despite thioacetamide being frequently used as the S precursor for cadmium chalcogenide and copper indium disulfide quantum dots,<sup>21,28,29</sup> opting for thioacetamide as the sulfur precursor to synthesize indium sulfide or zinc indium sulfide nanocrystals resulted in nanocrystals with sizes larger than the Bohr exciton radius.<sup>5,30–32</sup> As a consequence, quantum confinement effects and thus fluorescent indium sulfide and zinc indium sulfide nanocrystals cannot be observed.<sup>5,30,31</sup> In simpler terms, neither indium sulfide nor zinc indium sulfide colloidal quantum dots have been successfully synthesized using



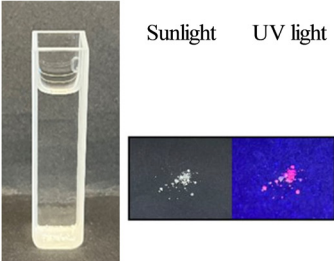
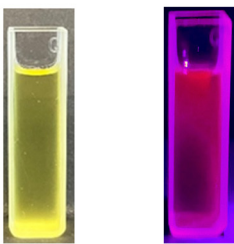
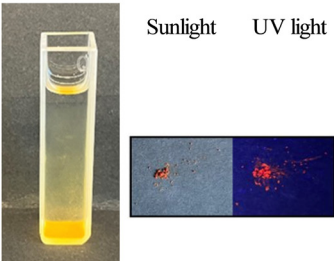
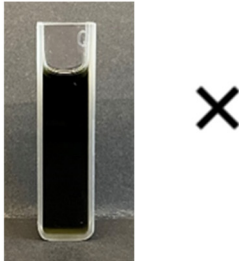
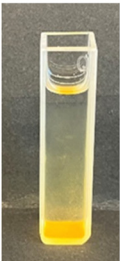

Sulfur Source	Capping Agent (1) Oleic Acid	Capping Agent (2) Oleylamine
1-dodecanethiol $\text{CH}_3(\text{CH}_2)_{11}\text{SH}$	Solid-State QDot 	Colloidal QDot Sunlight  UV light 
Thioacetamide $\text{CH}_3\text{CSNH}_2$	Solid-State QDot 	Colloidal QDot Sunlight  UV light 

Fig. 1 Observation of the state of ZCIS QDs (either colloidal or solid-state) with different capping agents (oleic acid and oleylamine) and sulfur precursor (1-dodecanethiol or thioacetamide). The color of each QD under sunlight and the fluorescence of each QD under UV-light (366 nm) are shown.

thioacetamide as the S precursor.<sup>5,30,31</sup> In this study, substituting the sulfur precursor from 1-dodecanethiol to thioacetamide by using oleylamine as the surfactant resulted in the formation of black colored solution without any precipitate, which did not display any sort of emissive properties (Fig. 1). It should be noted that initially all the syntheses were performed at 200 °C because when 1-dodecanethiol was used as the S precursor, the metal sulfide nanocrystals start to form above 200 °C;<sup>21</sup> however, high/fast reactivity of thioacetamide might cause overgrowth of nanocrystals,<sup>5,30,31</sup> thus in order to slow down the crystal growth, the temperature of the synthesis set-up was decreased to 150 °C, yet there was no indication of quantum dot formation. To sum up, only changing the S precursor to thioacetamide resulted in the formation of colloidal particles without any fluorescence properties, indicating that thioacetamide was not an ideal S precursor to synthesize colloidal indium-based quantum dots.

#### Effect of different sulfur precursors on fluorescence of CuInZnS SSQDs

To investigate the effect of different sulfur precursors on SSQDs, CuInZnS SSQDs were synthesized by using three sulfur sources: thioacetamide, 1-dodecanethiol (DDT) and 3-mercaptopropionic acid (3-MPA). Although each of these precursors resulted in the formation of QDs in solid-state matrices,

the brightness of the SSQDs synthesized with DDT and 3-MPA was lower compared to the brightness of CuInZnS SSQDs synthesized with thioacetamide (Fig. 2). Additionally, the full width at half maximum (FWHM) of the fluorescence peak collected from SSQDs increased significantly (35 nm for thioacetamide, 105 nm for 3-MPA, and 100 nm for DDT) (Fig. 2). The FWHM of the fluorescence spectrum can be regarded as a significant indicator of the size distribution of quantum dots. Due to the quantum confinement effect, the band gap between the valence and conduction bands of the quantum dots becomes dependent on the size of the quantum dots. As the size increases, the band gap decreases, and *vice versa*. As the fluorescence of a material is defined as the transition from the lowest vibrational level of the excited state to the ground state, the broadness of the fluorescence spectrum of quantum dots can be considered as evidence of the monodispersity or polydispersity of the size of quantum dots.<sup>33</sup> Therefore, the increase in the FWHM suggested the possible formation of SSQDs with polydispersed sizes. As a result, further experiments were conducted using thioacetamide as the sulfur precursor.

#### Synthesis of $\text{In}_2\text{S}_3$ , $\text{ZnIn}_2\text{S}_4$ and $\text{Cu:ZnIn}_2\text{S}_4$ SSQDs

Although colloidal copper indium disulfide (CIS) and zinc copper indium sulfide (ZCIS) QDs have been synthesized in various ways and extensively explored in the literature, the





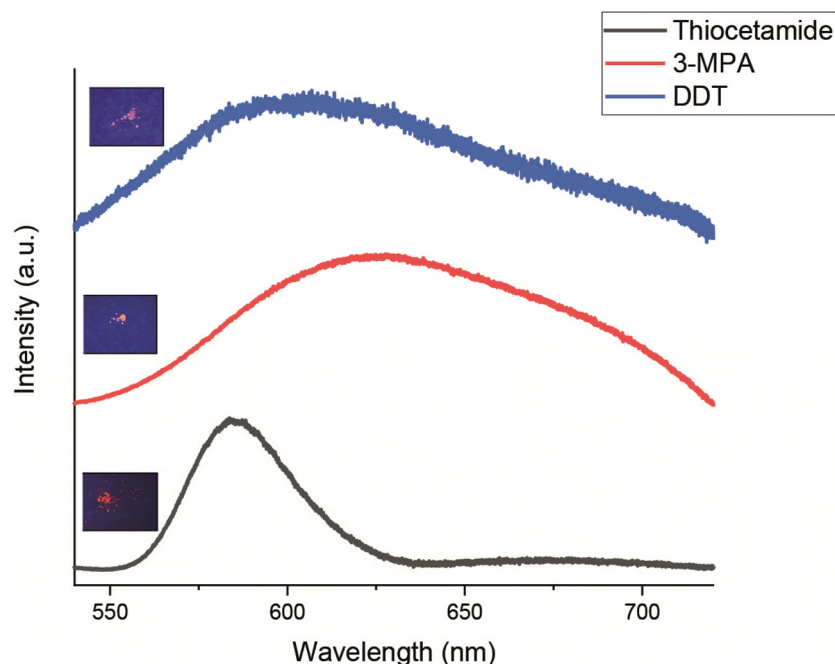


Fig. 2 Photoluminescence spectrum of CuInZnS SSQDs in which a sulfur precursor was used as thiocetamide, DDT and 3-MPA. The inset fluorescence pictures were taken under 366 nm UV-light.

synthesis of  $\text{In}_2\text{S}_3$  and  $\text{ZnIn}_2\text{S}_4$  QDs has received relatively little attention, with only a few studies conducted on these particles. However, it is important to note that  $\text{ZnIn}_2\text{S}_4$  is a particularly crucial material which is frequently used in various applications such as photocatalytic degradation of dyes and artificial photosynthesis solar cells.<sup>6,34</sup> The main reason why  $\text{ZnIn}_2\text{S}_4$  and  $\text{In}_2\text{S}_3$  QDs haven't garnered much research attention is the superior photophysical properties of CIS and ZCIS QDs, including a wide color gamut, high photoluminescence quantum yield, and high photostability, in contrast to the photophysical properties of  $\text{In}_2\text{S}_3$  and  $\text{ZnIn}_2\text{S}_4$  QDs.<sup>35,36</sup> In our study,  $\text{In}_2\text{S}_3$  and  $\text{ZnIn}_2\text{S}_4$  SSQDs were successfully synthesized with bright fluorescence intensity, particularly with  $\text{ZnIn}_2\text{S}_4$  SSQDs being the brightest among them all (Fig. 3).

#### Structural and elemental characterization of $\text{In}_2\text{S}_3$ , $\text{ZnIn}_2\text{S}_4$ and $\text{Cu:ZnIn}_2\text{S}_4$ SSQDs

To obtain more insight into the nature of SSQDs, the crystal structure, elemental composition and size of the quantum dots were determined by using X-ray diffraction (XRD), X-ray photoelectron spectroscopy (XPS), transmission electron microscopy (TEM) and Fourier transform infrared (FTIR) spectroscopy.

The size and size distribution of SSQDs were determined by TEM. The TEM analysis of solid-state materials showed that the SSQDs were trapped in solidified oleic acid matrices with a rough surface (Fig. 4). The TEM results of  $\text{In}_2\text{S}_3$  SSQDs showed that the QDs were dispersed in the solid structure and had an average size of 7 nm (see Fig. S2 for the size histogram of  $\text{In}_2\text{S}_3$  QDs dispersed in solid matrices, ESI†). The size of the  $\text{In}_2\text{S}_3$

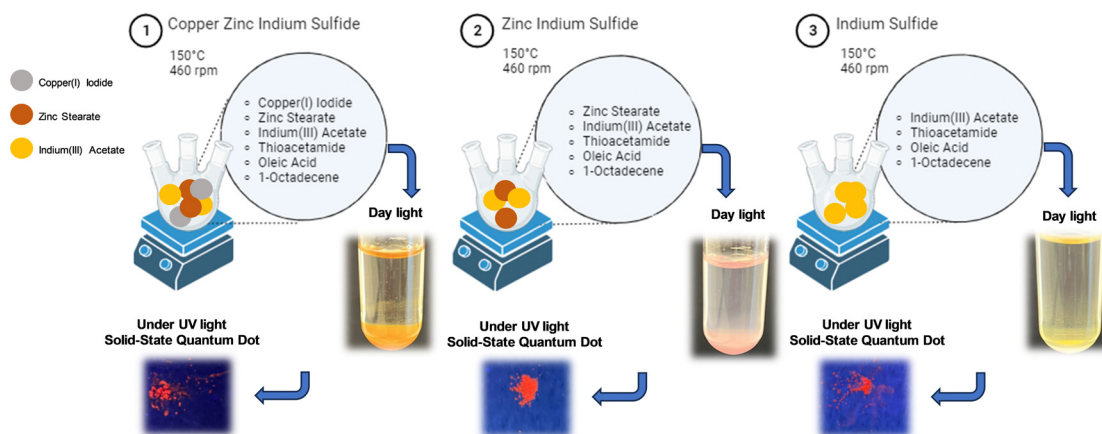


Fig. 3 Schematic illustration of the synthesis of  $\text{In}_2\text{S}_3$ ,  $\text{ZnIn}_2\text{S}_4$  and  $\text{Cu:ZnIn}_2\text{S}_4$  SSQDs.



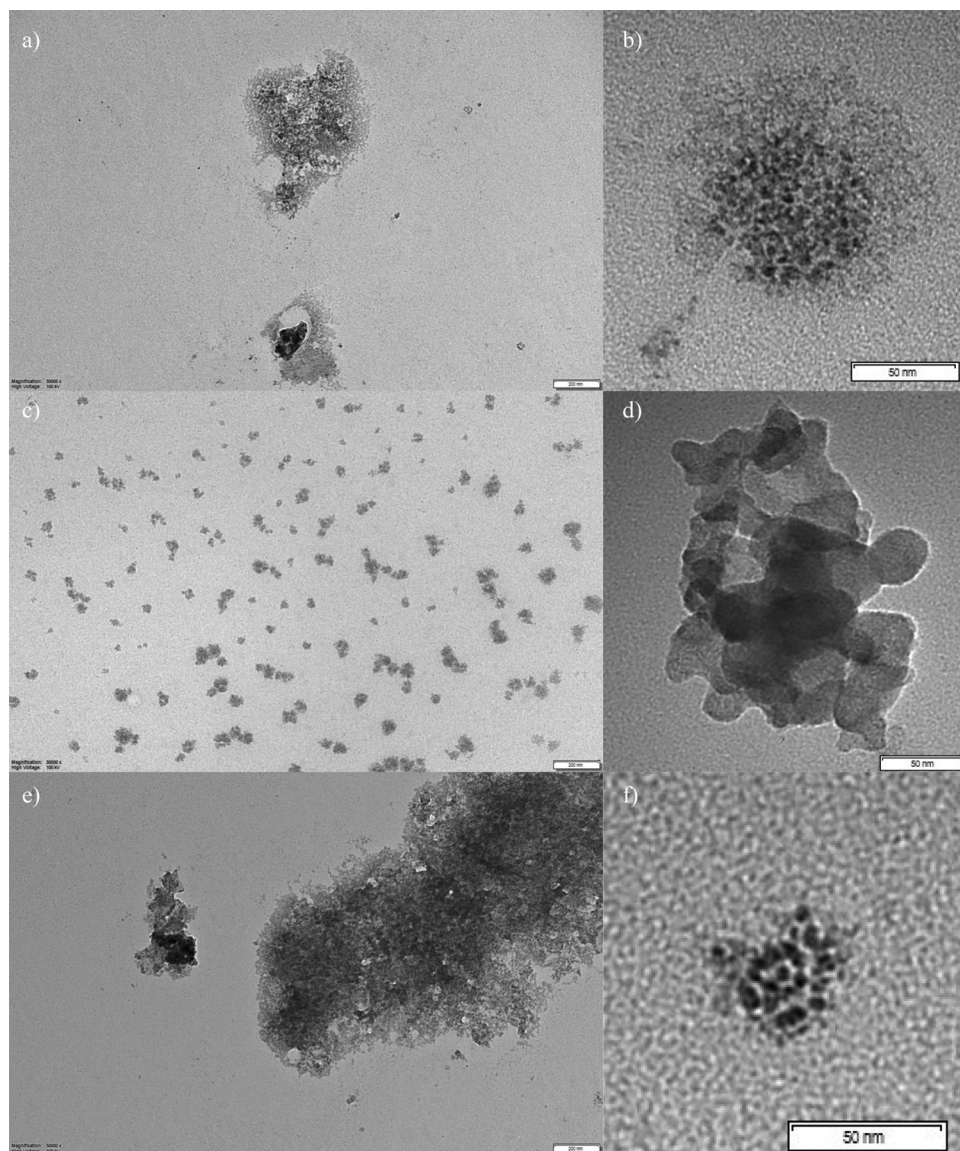


Fig. 4 TEM images of (a) and (b)  $\text{In}_2\text{S}_3$ , (c) and (d)  $\text{ZnIn}_2\text{S}_4$  and (e) and (f)  $\text{Cu:ZnIn}_2\text{S}_4$  SSQDs. The scale bar for (a), (c) and (e) is 200 nm. The scale bar for (b), (d) and (f) is 50 nm.

SSQDs was significantly lower than the Bohr exciton radius of  $\text{In}_2\text{S}_3$  (33 nm), which showed that the  $\text{In}_2\text{S}_3$  nanocrystals were within the quantum confinement regime.<sup>37,38</sup> As was observed for  $\text{In}_2\text{S}_3$  SSQDs, the TEM results showed that  $\text{ZnIn}_2\text{S}_4$  QDs were also dispersed in a solid structure and had an average size of 6 nm (Fig. 4, see Fig. S2 (ESI<sup>†</sup>) for the size histogram of  $\text{In}_2\text{S}_3$  SSQDs dispersed in solid matrices). It should be noted that even though the exact Bohr exciton radius of  $\text{ZnIn}_2\text{S}_4$  has not been exactly determined, the  $\text{ZnIn}_2\text{S}_4$  SSQDs show quantum confinement effects below 6 nm radius, and the  $\text{ZnIn}_2\text{S}_4$  SSQDs that were produced in this study were within the quantum confinement regime.<sup>6</sup> Also, the TEM results showed that  $\text{Cu:ZnIn}_2\text{S}_4$  SSQDs were dispersed in the solid structure and had an average size of 6 nm, which showed that the  $\text{Cu:ZnIn}_2\text{S}_4$  SSQDs were in the quantum confinement regime (Fig. 4, see Fig. S2

(ESI<sup>†</sup>) for the size histogram of  $\text{In}_2\text{S}_3$  SSQDs dispersed in solid matrices).<sup>6</sup>

The crystal structure of SSQDs was determined by XRD. The XRD pattern of  $\text{In}_2\text{S}_3$  SSQDs matched with the XRD pattern of cubic  $\text{In}_2\text{S}_3$  (JCPDS: card no. 05-00731 cubic  $\text{In}_2\text{S}_3$ )<sup>39</sup> but with significantly broadened peaks (Fig. 5). The identified planes for the  $\text{In}_2\text{S}_3$  peaks were as follows: (111) at  $2\theta$ : 27.3°, (200) at  $2\theta$ : 33.15°, (220) at  $2\theta$ : 47.9°, and the (311) plane at  $2\theta$ : 56.18°<sup>39</sup> (Fig. 5). The broadening of the peaks was a result of the nanosize of the  $\text{In}_2\text{S}_3$  SSQDs.<sup>39</sup> When the Zn precursor was added to the synthesis medium, a dramatic change in the crystal structure was observed, which suggested that a new type of crystal formed instead of Zn doped  $\text{In}_2\text{S}_3$  (Fig. 5). The most significant change was the disappearance of the (0012) peak in the XRD pattern of  $\text{In}_2\text{S}_3$  (Fig. 5). The new nanocrystal structure



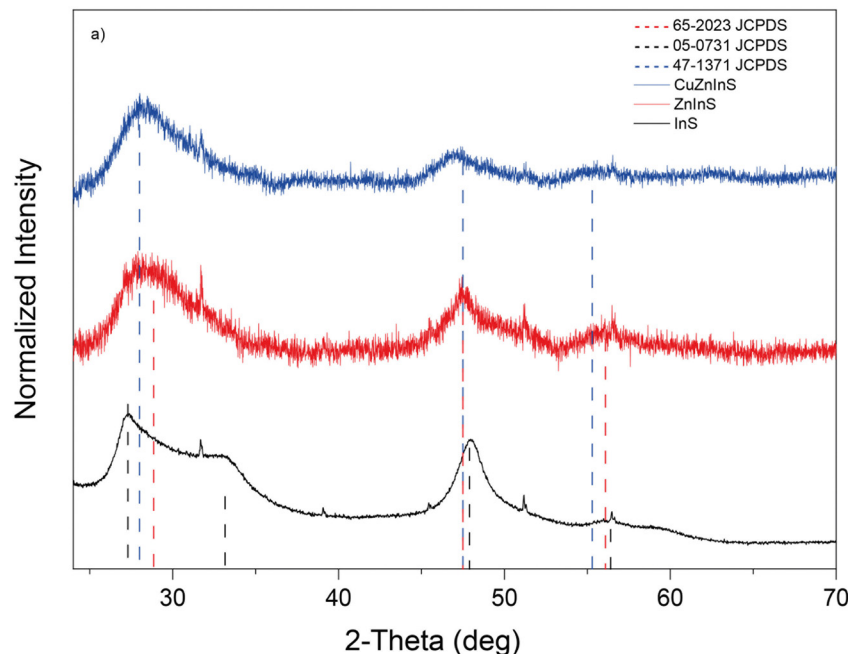


Fig. 5 (a) XRD spectra of  $\text{In}_2\text{S}_3$ ,  $\text{ZnIn}_2\text{S}_4$  and  $\text{Cu:ZnIn}_2\text{S}_4$  SSQDs (InS represents  $\text{In}_2\text{S}_3$ ,  $\text{ZnInS}$  represents  $\text{ZnIn}_2\text{S}_4$  and  $\text{CuZnInS}$  represents  $\text{Cu:ZnIn}_2\text{S}_4$ ).

matched with hexagonal  $\text{ZnIn}_2\text{S}_4$ , whose XRD characteristics were identified in the literature before<sup>4</sup> (JCPDS: card no. 65-2023 hexagonal  $\text{ZnIn}_2\text{S}_4$ ). The identified planes for the  $\text{ZnIn}_2\text{S}_4$  peaks were as follows: (101) at  $2\theta$ :  $28.85^\circ$ , (110) at  $2\theta$ :  $47.5^\circ$  and (202) at  $2\theta$ :  $56.1^\circ$  (Fig. 5). Similar to  $\text{In}_2\text{S}_3$ , the broadening of the  $\text{ZnIn}_2\text{S}_4$  peaks was a consequence of the nanosize of the SSQDs. Adversely, when the Cu precursor was added in addition to the Zn precursor, the XRD pattern of the new nanocrystal did not show a significant difference. The XRD peaks slightly shifted towards lower angles. This effect was expected since the XRD pattern of tetragonal  $\text{CuZnInS}$  had been observed at lower angles in the literature before<sup>40</sup> (JCPDS: 47-1371). These results indicated that the amount of Cu should be lower compared to the rest of the elements (Zn, In, and S) since there was no dramatic difference in the shape and position of the XRD peaks of  $\text{Cu:ZnIn}_2\text{S}_4$  (Fig. 5).

The elemental composition of each SSQD was determined by XPS measurements. According to the XPS results, the In:S atomic ratio in  $\text{In}_2\text{S}_3$  SSQDs was 2.3:3.4, the Zn:In:S atomic ratio in  $\text{ZnIn}_2\text{S}_4$  SSQDs was 1.1:1.9:3.7, and the Cu:Zn:In:S atomic ratio in  $\text{Cu:ZnIn}_2\text{S}_4$  SSQDs was 0.2:1.2:2.1:3.5 (Fig. 6). The atomic ratios of In:S in  $\text{In}_2\text{S}_3$  SSQDs and Zn:In:S in  $\text{ZnIn}_2\text{S}_4$  SSQDs were consistent with the XRD results (Fig. 6). Additionally, the atomic ratio of Cu in  $\text{Cu:ZnIn}_2\text{S}_4$  SSQDs was relatively low, which indicated that Cu was a dopant in  $\text{Cu:ZnIn}_2\text{S}_4$  SSQDs and this result was in line with the XRD pattern of  $\text{Cu:ZnIn}_2\text{S}_4$  QDs (Fig. 5 and 6). The HR-XPS spectra of the common elements in the SSQD structures, In(3d) and S(2p), indicated that the bonding characteristics of In and S were different in each SSQD (Fig. 6). The HR-XPS peak of S(2p) composed of 2 peaks merged into each other for each QD; one peak at a high energy region which corresponds to  $2p_{3/2}$  (162.6 eV for  $\text{In}_2\text{S}_3$  and 163.1 eV for  $\text{ZnIn}_2\text{S}_4$  and  $\text{Cu:ZnIn}_2\text{S}_4$ )

accompanied by another peak at a lower energy region which corresponds to  $2p_{1/2}$  (161.4 eV for  $\text{In}_2\text{S}_3$  and 161.9 eV for  $\text{ZnIn}_2\text{S}_4$  and  $\text{Cu:ZnIn}_2\text{S}_4$ ). Both of these peaks shifted towards a higher energy region in  $\text{ZnIn}_2\text{S}_4$  and  $\text{Cu:ZnIn}_2\text{S}_4$  SSQDs compared to  $\text{In}_2\text{S}_3$  SSQDs (see the ESI† for the deconvoluted HR-XPS S(2p) spectrum for each SSQD, Fig. S3). This observation was expected due to the higher electronegativity (EN) difference between Zn (EN = 1.6) and S (EN = 2.5) compared to the EN difference between In (EN = 1.7) and S (Fig. 6). Furthermore, the  $3d_{5/2}$  and  $3d_{3/2}$  peaks (appeared at 452.5 eV and 445.1 eV, respectively) in the HR-XPS spectrum of In(3d) broadened in  $\text{ZnIn}_2\text{S}_4$  and  $\text{Cu:ZnIn}_2\text{S}_4$  SSQDs (the FWHM of the  $3d_{5/2}$  peak: 1.1 eV for  $\text{In}_2\text{S}_3$  and 1.4 eV for  $\text{ZnIn}_2\text{S}_4$  and  $\text{Cu:ZnIn}_2\text{S}_4$  and the FWHM of the  $3d_{3/2}$  peak: 1.1 eV for  $\text{In}_2\text{S}_3$  and 1.6 eV for  $\text{ZnIn}_2\text{S}_4$  and  $\text{Cu:ZnIn}_2\text{S}_4$ ) since the presence of Zn affected the bonding characterization of In by creating an extra interaction and led to broadening in the XPS peaks (Fig. 6). As the HR-XPS of C(1s) was investigated, it was observed that the C=O peak around 288 eV almost disappeared. The HR-XPS of C(1s) displayed a single-narrow peak at 284.9 eV, which belonged to  $sp^3$  hybridized carbons.<sup>41</sup> The HR-XPS spectrum of C(1s) revealed that the  $sp^3$  hybridized carbons dominated the structure and the presence of  $sp^2$  hybridized carbons was almost insignificant (the XPS peak of  $sp^2$  hybridized carbons should be around 284 eV). This result indicated that the double bond in oleic acid, an unsaturated fatty acid, was most probably broken and may lead to the formation of a cross-linked structure, which was observed for a different type of quantum dot before in the literature.<sup>25</sup>

The FTIR spectrum of  $\text{In}_2\text{S}_3$ ,  $\text{ZnIn}_2\text{S}_4$  SSQDs and  $\text{Cu:ZnIn}_2\text{S}_4$  SSQDs displayed similar characteristics, indicating that these quantum dots had comparable surface properties. In order to understand the solid nature of the material, the FTIR spectra of





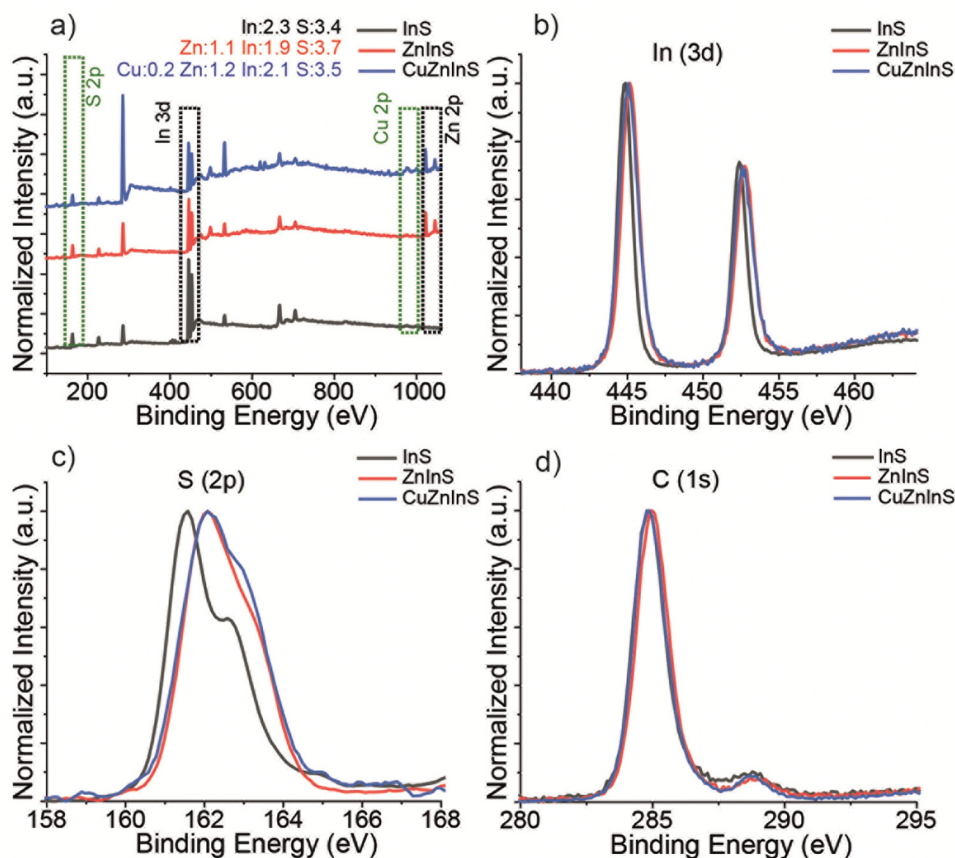


Fig. 6 (a) XPS survey spectra of In<sub>2</sub>S<sub>3</sub>, ZnIn<sub>2</sub>S<sub>4</sub> and Cu:ZnIn<sub>2</sub>S<sub>4</sub> SSQDs. (b) HR-XPS survey spectra of (b) In(3d), (c) S(2p) and (d) C(1s) spectra of In<sub>2</sub>S<sub>3</sub>, ZnIn<sub>2</sub>S<sub>4</sub> and Cu:ZnIn<sub>2</sub>S<sub>4</sub> SSQDs (InS represents In<sub>2</sub>S<sub>3</sub>, ZnInS represents ZnIn<sub>2</sub>S<sub>4</sub> and CuZnInS represents Cu:ZnIn<sub>2</sub>S<sub>4</sub>).

SSQDs (Fig. S4, ESI<sup>†</sup>) were compared with the FTIR spectrum of colloidal oleic acid capped CdSeS QDs (Fig. S5, ESI<sup>†</sup>). The disappearance of the hydroxyl (–OH) peak at around 3100–3400 cm<sup>−1</sup> indicated that oleic acid surrounded the QDs through the carboxyl group (Fig. S4, ESI<sup>†</sup>).<sup>25,42</sup> Another noteworthy observation was the disappearance of the C=O peak of the carboxylate group at 1700 cm<sup>−1</sup>, suggesting that carboxyl groups interacted with metals within the quantum dots (Fig. S4, ESI<sup>†</sup>).<sup>25,42</sup> Also, the C=C peak, which arose around 3000–3020 cm<sup>−1</sup> in the FTIR spectrum of CdSeS QDs (Fig. S4, ESI<sup>†</sup>), disappeared while an increase in the band around 1000–1100 cm<sup>−1</sup> that corresponds to C–C bonds was observed (Fig. S4, ESI<sup>†</sup>). It should be noted that the band around 1000–1100 cm<sup>−1</sup> was not observed in the FTIR spectrum of oleic acid capped CdSeS QDs (Fig. S5, ESI<sup>†</sup>). These results were in line with the XPS results of C (1s). In short, these observations supported the XPS data and suggested the formation of a cross-linked structure which was observed in the literature before for different types of QDs<sup>25</sup> and oleic acid alone,<sup>26</sup> which would explain the insoluble nature for In based SSQDs.

#### Optical characterization of In<sub>2</sub>S<sub>3</sub>, ZnIn<sub>2</sub>S<sub>4</sub> and Cu:ZnIn<sub>2</sub>S<sub>4</sub> SSQDs in solid-state oleic acid matrices

The temporal evolution of SSQDs was observed on analysing the absorption spectrum of each quantum dot at different time

intervals. The SSQDs displayed typical absorption behaviour of traditional SSQDs; each quantum dot had a broad absorption spectrum with a characteristic shoulder that corresponds to crystal band-edge transition (Fig. 7). The band-edge peak is slightly shifted to a lower energy region as Zn and Cu were incorporated into the SSQD structure; the position of the peak was 574 nm for In<sub>2</sub>S<sub>3</sub>, 577 nm for ZnIn<sub>2</sub>S<sub>4</sub> and 580 nm for Cu:ZnIn<sub>2</sub>S<sub>4</sub>. In order to observe the growth of SSQDs over time, the shift of the band-edge transition peak with respect to different experiment times was checked (Fig. 7). In theory, the SSQDs should increase with longer synthesis time and as a consequence of the quantum confinement effect, the band-edge transition peak should red-shift with the increase of SSQDs.<sup>43</sup> In our study, the band-edge transition peak shifted slightly towards longer wavelengths as the synthesis time increased, as expected (Fig. 7).

The SSQDs synthesized in this study exhibited insolubility in both polar and non-polar solvents. They were insoluble in their synthesis solvent, 1-octadecene, as well as other solvents with varying polarities such as toluene, chloroform, acetone, dimethylsulfoxide, *N,N*-dimethylformamide, tetrahydrofuran, methanol, ethanol, and water. Therefore, the photoluminescence spectra of the SSQDs were obtained from the solid product using Raman microscopy with an excitation wavelength of 532 nm (Fig. 7). The excitation wavelength was





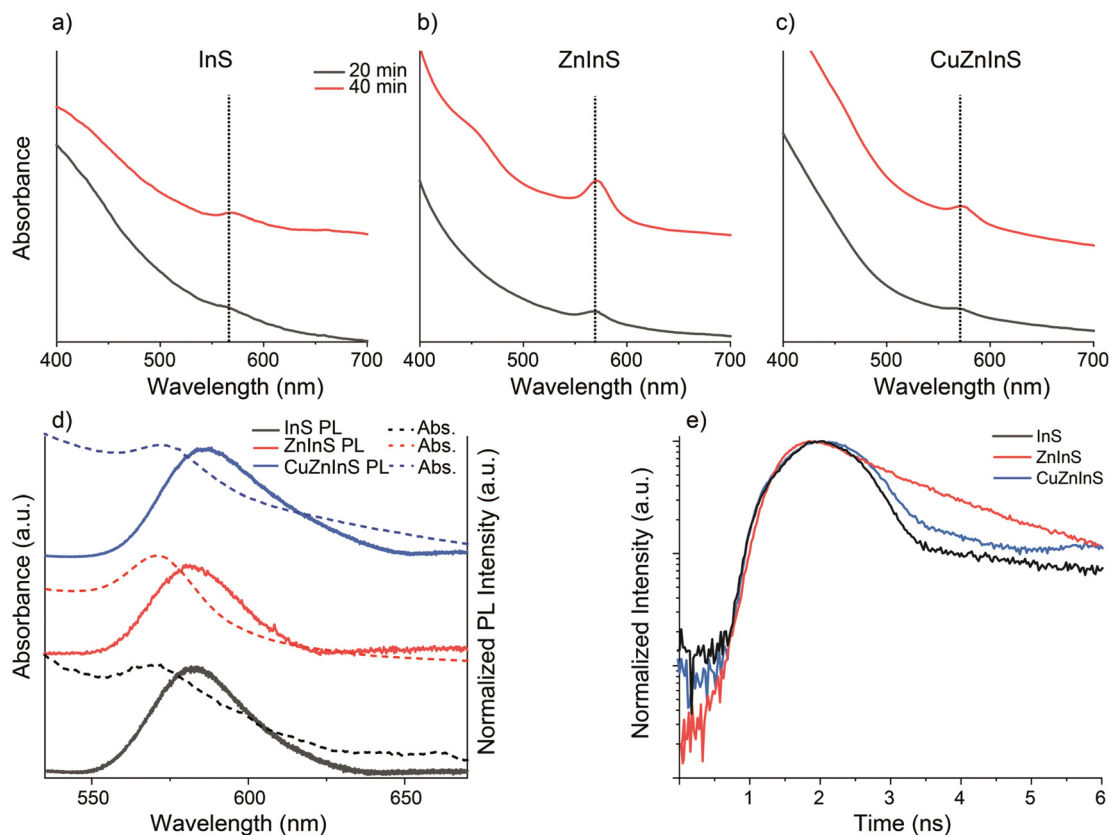


Fig. 7 Absorption spectrum of solid-state (a)  $\text{In}_2\text{S}_3$ , (b)  $\text{ZnIn}_2\text{S}_4$  and (c)  $\text{Cu:ZnIn}_2\text{S}_4$  SSQDs at 20 minutes (black) and 40 minutes (red) after synthesis started. The synthesis was ended at 40<sup>th</sup> minute for each SSQD. The dotted line represents the peak point of the band-edge transition band at 20<sup>th</sup> minute. (d) Photoluminescence (PL, solid line) and absorption (Abs., dotted line) spectra of  $\text{In}_2\text{S}_3$ ,  $\text{ZnIn}_2\text{S}_4$  and  $\text{Cu:ZnIn}_2\text{S}_4$  SSQDs. PL emission was collected at 532 nm excitation wavelength. (e) Time-resolved fluorescence decays of  $\text{In}_2\text{S}_3$ ,  $\text{ZnIn}_2\text{S}_4$  and  $\text{Cu:ZnIn}_2\text{S}_4$  SSQDs ( $\text{InS}$  represents  $\text{In}_2\text{S}_3$ ,  $\text{ZnInS}$  represents  $\text{ZnIn}_2\text{S}_4$  and  $\text{CuZnInS}$  represents  $\text{Cu:ZnIn}_2\text{S}_4$ ).

decided with respect to the band-edge absorption peak of SSQDs (Fig. 7). Additionally, the emission of SSQDs was visualized under an excitation wavelength of 366 nm, within the typical excitation wavelength range for QDs,<sup>22,23,44</sup> resulting in an orange color emission for each SSQD (Fig. 7). Upon 532 nm excitation, the  $\text{In}_2\text{S}_3$  SSQDs exhibited a single emission peak around 580 nm. The emission peak of  $\text{ZnIn}_2\text{S}_4$  SSQDs slightly shifted towards longer wavelengths, appearing at 583 nm. The addition of Cu caused an additional red-shift in the emission peak of  $\text{Cu:ZnIn}_2\text{S}_4$  SSQDs, which appeared at 586 nm. Similar behaviour was observed in the absorption spectrum of SSQDs; integration of Zn caused a slight red-shift in the band-edge transition peak in the absorption spectrum, while integration of Cu to  $\text{ZnInS}$  caused even further shift towards the lower energy region in the band-edge transition peak in the absorption spectrum. The fluorescence quantum yields of the SSQDs were measured as follows: 31.73% for  $\text{ZnIn}_2\text{S}_4$  QDs, 4.74% for  $\text{Cu:ZnIn}_2\text{S}_4$  SSQDs and below 1% for  $\text{In}_2\text{S}_3$  SSQDs (see Fig. S6, ESI†). As the fluorescence decays of SSQDs were observed, it was found that the  $\text{ZnIn}_2\text{S}_4$  SSQDs possessed the longest average fluorescence lifetime (1.34 ns). The average fluorescence lifetimes of  $\text{Cu:ZnIn}_2\text{S}_4$  SSQDs and  $\text{In}_2\text{S}_3$  SSQDs were 0.704 ns and 0.540 ns, respectively. The fluorescence lifetimes of SSQDs were coherent with the quantum yields of SSQDs; as

the quantum yield of the SSQD decreased, the fluorescence lifetime of the SSQD became shorter. The fluorescence decay of  $\text{ZnIn}_2\text{S}_4$  SSQDs was monoexponential, indicating that mainly a single radiative process took place. However, the fluorescence decays of  $\text{Cu:ZnIn}_2\text{S}_4$  QDs and  $\text{In}_2\text{S}_3$  SSQDs were biexponential with a fast-dominant component (for  $\text{Cu:ZnIn}_2\text{S}_4$ ; 0.614 ns with an amplitude of 82% and 1.127 ns with an amplitude of 18%, for  $\text{In}_2\text{S}_3$ ; 0.425 ns with an amplitude of 92% and 1.190 ns with an amplitude of 8%), suggesting that a fast radiative process took place in these QDs resulting in a decrease in the quantum yield.

### Thermoresponsive properties of $\text{ZnIn}_2\text{S}_4$ SSQDs

The thermal response of fluorescence of colloidal quantum dots has been widely studied in the literature.<sup>18–20</sup> Yet, to date, quantum dots have been rarely tested as a potential temperature sensor in solid-state materials as they display different photophysical properties in colloidal and aggregate forms.<sup>18–20</sup> In our study, the  $\text{ZnInS}$  SSQDs in solid-state matrices displayed thermoresponsive properties while others did not. To investigate the response of  $\text{ZnIn}_2\text{S}_4$  SSQDs to different temperatures, a heating experiment was conducted, and the photoluminescence of the SSQDs under UV-light was monitored (Fig. 8). The emission of  $\text{ZnIn}_2\text{S}_4$  QDs was examined at various



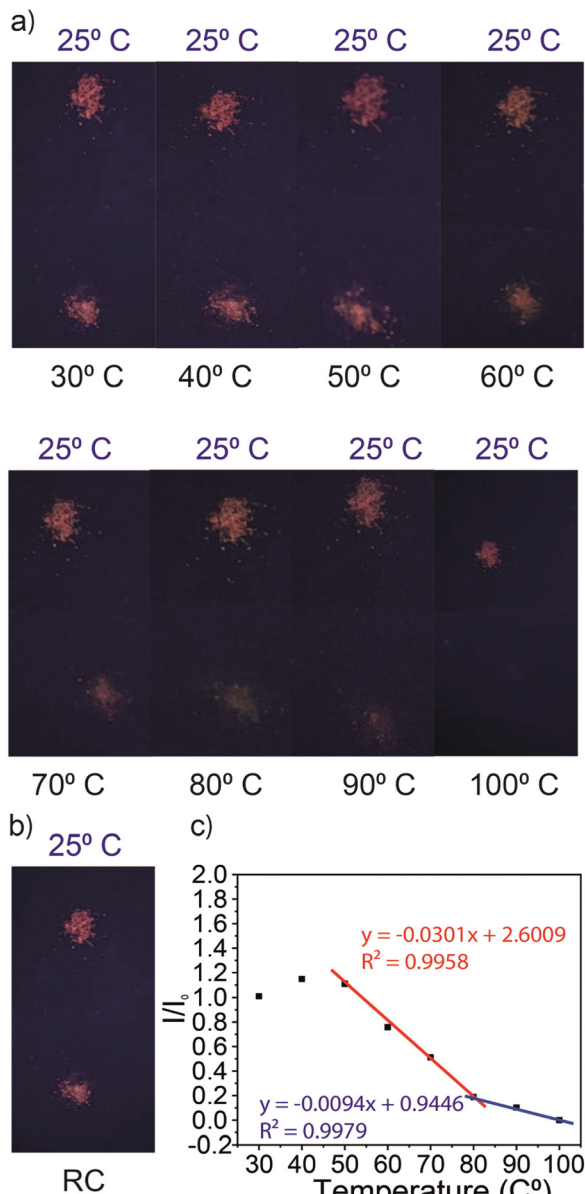


**Fig. 8** (a) Change of the emission intensity of  $\text{ZnIn}_2\text{S}_4$  SSQDs at different temperatures. The solid structures on the bottom are SSQDs at different temperatures, and the solid structures on the top are SSQDs remained at room temperature. Both of them displayed in the same image to reflect the decrease in the fluorescence. The abbreviation RC was used to show the recovery of the fluorescence after cooling of the solids (b). The quantum dots were excited using UV-light (366 nm). (c) The change of the fluorescence intensity of  $\text{ZnIn}_2\text{S}_4$  SSQDs as a function of temperature.  $I$  = the fluorescence intensity at target temperature and  $I_0$  = the fluorescence intensity at 25 °C.

temperatures ranging from 25 °C to 100 °C (Fig. 8). Up to 50 °C, there was no observable change in the intensity and color of the fluorescence of  $\text{ZnIn}_2\text{S}_4$  QDs (Fig. 8). However, beyond 50 °C, a gradual decrease in the fluorescence intensity was observed as the temperature increased (Fig. 8). At 100 °C, the fluorescence of  $\text{ZnIn}_2\text{S}_4$  QDs was completely quenched (Fig. 8). Remarkably, when the quenched  $\text{ZnIn}_2\text{S}_4$  SSQDs were brought back to room

temperature which were heated up to 160 °C, their fluorescence recovered within seconds (Fig. 8). Conversely, when the  $\text{ZnIn}_2\text{S}_4$  SSQDs were heated beyond 160 °C, the recovery of fluorescence was not observed, and the quenching of fluorescence became permanent.

As the quenching of fluorescence with respect to the increase in temperature was checked, it was observed that the fluorescence intensity of  $\text{ZnIn}_2\text{S}_4$  SSQDs decreased linearly between 50 °C and 100 °C (Fig. 8). The decrease between 50 °C and 80 °C was steeper compared to the decrease between 80 °C and 100 °C (Fig. 8). This observation showed that the conversion rate between the fluorescence state and quenched state of  $\text{ZnIn}_2\text{S}_4$  SSQDs was faster between 50 °C and 80 °C; however, this conversion rate slowed down as the temperature increased and  $\text{ZnIn}_2\text{S}_4$  SSQDs were completely converted to the quenched state at 100 °C (Fig. 8). In order to understand the mechanism behind the quenching, several experiments were conducted at 70 °C. The fluorescence recovery of SSQDs at room temperature was within seconds ( $\sim 5$  seconds) which was a proof of the intact structure of nanocrystals in the SSQD structure (see the Video in the ESI†). The fluorescence of SSQDs increases because of the quantum confinement effect that nanocrystals undergo; therefore the recovery of fluorescence was an indication of the stable structure of nanocrystals. As the quantum yields of the SSQDs were measured, it was observed that the quantum yield of the SSQD was dropped to 3% (Fig. S7, ESI†). A fluorescence lifetime experiment on SSQDs at 70 °C was carried out in order to comprehend the decrease in the quantum yield. At this temperature, there was a noticeable change in the fluorescence decay: instead of being monoexponential, it became biexponential as a result of the formation of a fast decay component (Fig. S8, ESI†). This finding implied that the electrons of SSQDs underwent a transition to a different vibrational energy level during heating, which prevented the formation of fluorescence. Upon cooling, this transition was cancelled and the fluorescence was recovered.

As was mentioned before, this conversion was reversible up to 160 °C. After 160 °C, the conversion was irreversible and QDs became permanently quenched. To investigate the reason behind the permanent quenching of  $\text{ZnIn}_2\text{S}_4$  QDs, the X-ray diffraction (XRD) pattern of  $\text{ZnIn}_2\text{S}_4$  SSQDs following permanent quenching was examined (Fig. S9, ESI†). The crystallinity of  $\text{ZnIn}_2\text{S}_4$  SSQDs treated at 200 °C exhibited significant differences (Fig. S9, ESI†). The intensity of the characteristic  $\text{ZnIn}_2\text{S}_4$  XRD peaks decreased considerably upon heating up to 200 °C (Fig. S6, ESI†). These results indicated that as the temperature increased, the  $\text{ZnIn}_2\text{S}_4$  SSQD crystal structure started to be defected and consequently, the fluorescence of the SSQDs, which arose from their nanocrystal characteristics due to the quantum confinement effect, quenched.

### Micropollutant removal from aqueous medium

The quantum dots trapped in solid-state matrices were also tested for their potential to remove various micropollutants from aqueous environments. In the literature, indium-incorporated cage structures, such as indium-incorporated



MOFs or COFs, have frequently been used in dye adsorption studies, particularly for cationic dyes.<sup>8–12</sup> Additionally, specifically modified cross-linked structures have been proposed as potential agents for removing dyes due to their insoluble, solid, and porous nature.<sup>45</sup> In our study,  $\text{In}_2\text{S}_3$ ,  $\text{ZnIn}_2\text{S}_4$ , and  $\text{Cu:ZnIn}_2\text{S}_4$  SSQDs were employed as removal agents to eliminate several different cationic and anionic dyes from their aqueous solutions. Methylene blue, methyl violet 2B, and rhodamine B were selected as cationic dyes, while methyl orange and sodium fluorescein were chosen as anionic dyes.

When aqueous solutions of cationic dyes were agitated with SSQDs, the color of the solutions faded, especially when  $\text{In}_2\text{S}_3$  was used, which almost completely removed methylene blue from its aqueous solution (Fig. 9). Also, SSQDs were quenched upon interaction, which showed that nanocrystals in the solid state matrices were mainly interacting with dyes (Fig. S10, ESI†). To understand the extent of the removal, the removal efficiencies for dyes were calculated (Table 1).

The removal efficiency ( $R$ ) of each SSQD for each dye was calculated by using the following equation:

$$R = \frac{c_0 - c_e}{c_0} \times 100\%$$

where  $c_0$  (mM) is the initial dye concentration and  $c_e$  (mM) is the dye concentration after SSQD treatment.

In terms of cationic dye removal efficiency,  $\text{In}_2\text{S}_3$  exhibited the highest performance for methylene blue and methyl violet 2b (Table 1). For rhodamine B,  $\text{Cu:ZnIn}_2\text{S}_4$  SSQDs displayed the highest removal efficiency (Table 1). Additionally,  $\text{ZnIn}_2\text{S}_4$  SSQDs showed notably high removal efficiencies when removing cationic dyes from aqueous solutions (Table 1).

In contrast, the anionic dyes  $\text{ZnIn}_2\text{S}_4$  and  $\text{Cu:ZnIn}_2\text{S}_4$  SSQDs did not significantly remove the micropollutants from their

**Table 1** The removal efficiencies of SSQDs for each dye. Abbreviations for the dyes: methylene blue (MB), methyl violet 2B (MV), rhodamine B (RB), methyl orange (MO), and sodium fluorescein (NF)

	MB (%)	MV (%)	RB (%)	MO (%)	NF (%)
$\text{In}_2\text{S}_3$ SSQDs	98.9	95.0	66.5	42.1	38.4
$\text{ZnIn}_2\text{S}_4$ SSQDs	56.1	79.7	59.5	8.6	8.6
$\text{Cu:ZnIn}_2\text{S}_4$ SSQDs	51.9	93.7	82.1	7.5	12.1

aqueous solutions (Fig. 10). On the other hand,  $\text{In}_2\text{S}_3$  exhibited considerable efficiency in removing both methyl orange and sodium fluorescein (Table 1). These findings suggest that  $\text{In}_2\text{S}_3$  SSQDs hold significant promise as a micropollutant removal agent for water treatment (Table 1). Furthermore,  $\text{ZnIn}_2\text{S}_4$  and  $\text{Cu:ZnIn}_2\text{S}_4$  SSQDs can be utilized for removing anionic dyes from aqueous solutions.

It should be noted that particularly when it comes to treating dye-related wastewater, indium-based materials have shown great promise for adsorption research.<sup>8–12</sup> For example, indium-based metal-organic frameworks (In-MOFs) exhibited remarkable adsorption efficiency for a variety of cationic dyes, including methylene blue, azure A, and others.<sup>8,9</sup> Furthermore, materials such as indium-based mesoporous adsorbents exhibited better adsorption capabilities and improved efficiency for dyes like methylene blue and basic yellow-28 due to the structural incorporation of indium atoms.<sup>10</sup> Moreover, the removal of rhodamine B from water demonstrates how indium enhances adsorption performance when combined with other materials, such as graphite oxide in the In-MOF@GO composite.<sup>11</sup> In comparison to the conventional In-MOF, the addition of graphene oxide to the composite greatly increases adsorption activity, making it a viable wastewater treatment solution.<sup>11</sup> To sum up, the remarkable adsorption properties of

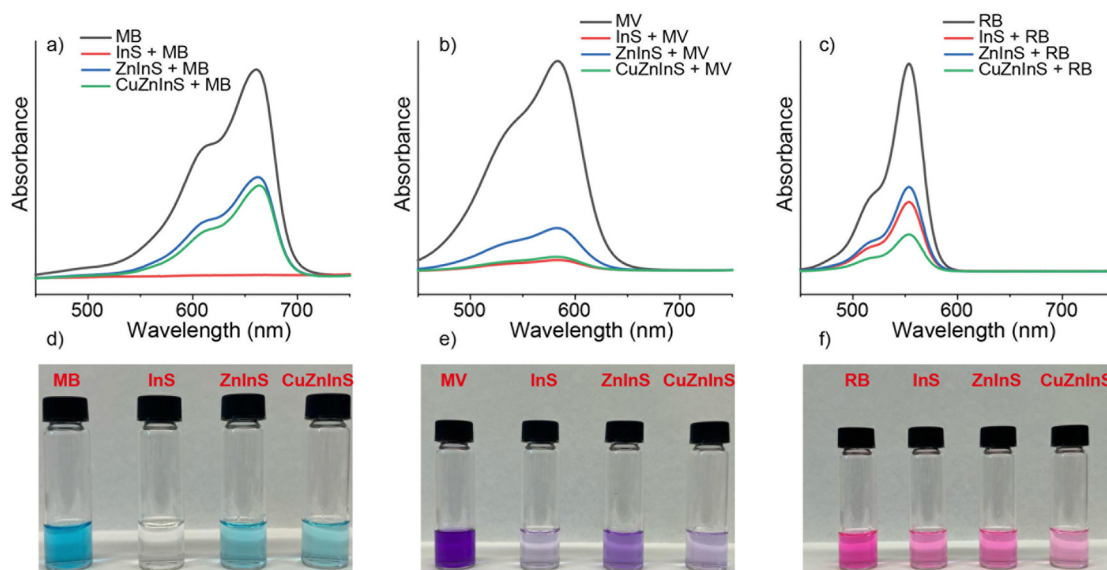


**Fig. 9** Removal of cationic organic dyes with SSQDs. Absorption spectra of dyes and SSQD + dye solutions after 1 day of shaking for (a) methylene blue (MB), (b) methyl violet 2B (MV) and (c) rhodamine B (RB). The images represent dyes and SSQD + dye solutions after 1 day of shaking for (d) methylene blue (MB), (e) methyl violet 2B (MV) and (f) rhodamine B (RB) (InS represents  $\text{In}_2\text{S}_3$ , ZnInS represents  $\text{ZnIn}_2\text{S}_4$  and CuZnInS represents  $\text{Cu:ZnIn}_2\text{S}_4$ ).





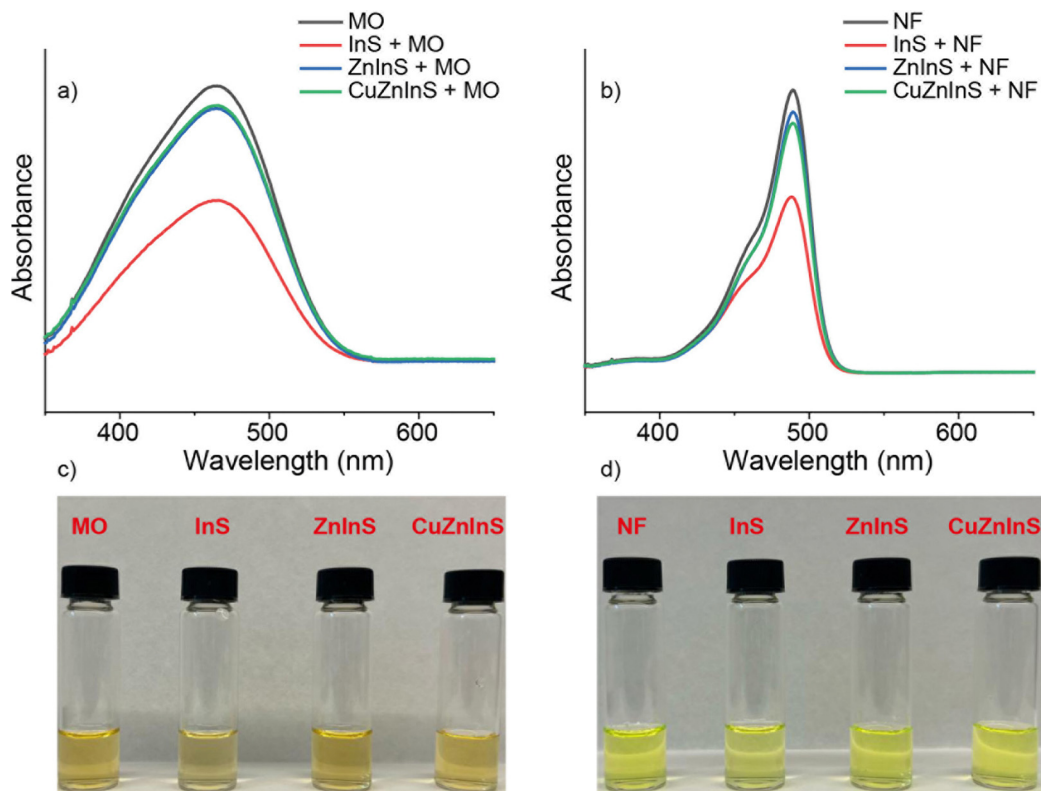


**Fig. 10** Removal of anionic organic dyes with SSQDs. Absorption spectra of dyes and SSQD + dye solutions after 1 day of shaking for (a) methyl orange (MO) and (b) sodium fluorescein (NF). The images represent dyes and SSQD + dye solutions after 1 day of shaking for (c) methyl orange (MO) and (d) sodium fluorescein (NF) (InS represents  $\text{In}_2\text{S}_3$ , ZnInS represents  $\text{ZnIn}_2\text{S}_4$  and CuZnInS represents  $\text{Cu:ZnIn}_2\text{S}_4$ ).

materials based on indium originate from their structural features, which offer a multitude of active sites for interactions with molecules of dyes. On the other hand, when zinc and copper were incorporated into the structure, additional interactions would occur between SSQDs and dyes which would affect the adsorption capacity of the SSQDs. Other than rhodamine B, all the adsorption capacities decreased upon these interactions.

## Conclusions

In conclusion, a one-pot single-step synthesis technique to create solid-state matrices incorporating  $\text{In}_2\text{S}_3$ ,  $\text{ZnIn}_2\text{S}_4$ , and  $\text{Cu:ZnIn}_2\text{S}_4$  SSQDs, which were trapped in oleic acid, was utilized. These SSQDs, ranging in size from 4 nm to 7 nm, were dispersed within a solidified network formed by surfactant molecules, rendering them insoluble in any type of solvent. The SSQDs emitted fluorescence in the wavelength range of 580–586 nm (which could be finely tuned by controlling the chemical composition) with a notably high fluorescence quantum yield, reaching up to 31%. These SSQDs possessed an average fluorescence lifetime between 1.34 ns and 0.540 ns. Remarkably, the  $\text{ZnIn}_2\text{S}_4$  SSQDs exhibited a distinctive thermo-responsive behavior. Upon heat exposure, the fluorescence of  $\text{ZnIn}_2\text{S}_4$  SSQDs gradually diminished until reaching 100 °C, completely extinguishing at this point. Between 100 °C and

160 °C, the decrease in fluorescence was reversible, allowing for recovery at room temperature. However, beyond 160 °C, the fluorescence recovery was no longer observed. Additionally, the indium-based SSQDs demonstrated significant potential in water decontamination from organic micropollutants. All synthesized SSQDs displayed notably high removal efficiency against cationic organic dyes (such as methylene blue, methyl violet 2B, and rhodamine B). Specifically,  $\text{In}_2\text{S}_3$  SSQDs exhibited remarkable efficiency in removing anionic dyes (methyl orange and sodium fluorescein).

## Conflicts of interest

There are no conflicts to declare.

## Acknowledgements

The authors thank Ege University – Central Research Test and Analysis Laboratory Application and Research Center (EGE-MATAL) for the XPS measurements. The fluorescence quantum yield and fluorescence lifetime measurements were conducted at KUYTAM – Koç University Surface Science and Technology Center. This work was supported by the TÜBİTAK (The Scientific and Technological Research Council of Turkey) under The Scientific and Technological Research Projects Funding Program (programme no. 2244) [grant number: 119C197].





## References

- 1 P. M. Allen and M. G. Bawendi, *J. Am. Chem. Soc.*, 2008, **130**, 9240–9241.
- 2 Y. H. Won, O. Cho, T. Kim, D. Y. Chung, T. Kim, H. Chung, H. Jang, J. Lee, D. Kim and E. Jang, *Nature*, 2019, **575**, 634–638.
- 3 L. Li, T. J. Daou, I. Texier, T. T. K. Chi, N. Q. Liem and P. Reiss, *Chem. Mater.*, 2009, **21**, 2422–2429.
- 4 J. Wang, Y. Chen, W. Zhou, G. Tian, Y. Xiao, H. Fu and H. Fu, *J. Mater. Chem. A*, 2017, **5**, 8451–8460.
- 5 X. Wang, J. Damasco, W. Shao, Y. Ke and M. T. Swihart, *ChemPhysChem*, 2016, **17**, 687–691.
- 6 Y. Pan, X. Yuan, L. Jiang, H. Yu, J. Zhang, H. Wang, R. Guan and G. Zeng, *Chem. Eng. J.*, 2018, **354**, 407–431.
- 7 Z. Long, W. Zhang, J. Tian, G. Chen, Y. Liu and R. Liu, *Inorg. Chem. Front.*, 2021, **8**, 880–897.
- 8 K. Maru, S. Kalla, A. K. Ghosh and R. Jangir, *Res. Chem. Intermed.*, 2024, **50**, 147–174.
- 9 L. Feng, X. Zhang, Z. Jin, J. Chen, X. Duan, S. Ma and T. Xia, *Molecules*, 2023, **28**, 4980.
- 10 R. K. Khaled, M. A. Wahba, M. D. Badry, M. F. Zawrah and E. A. Heikal, *J. Mater. Sci.*, 2022, **57**, 4504–4527.
- 11 C. Yang, S. Wu, J. Cheng and Y. Chen, *J. Alloys Compd.*, 2016, **687**, 804–812.
- 12 P. Huang, C. Chen, M. Wu, F. Jiang and M. Hong, *Dalton Trans.*, 2019, **48**, 5527–5533.
- 13 S. M. Aminossadati, N. M. Mohammed and J. Shemshad, *Tunn. Undergr. Sp. Technol.*, 2010, **25**, 220–229.
- 14 D. Chenyu, *J. Phys.: Conf. Ser.*, 2021, **2005**, 012113.
- 15 A. C. Benniston, G. Copley, A. Harriman and R. Ryan, *J. Mater. Chem.*, 2011, **21**, 2601–2608.
- 16 P. Yao, W. Qiao, Y. Wang, H. Peng, X. Xie and Z. Li, *Chem. – Eur. J.*, 2022, **28**, e202200725.
- 17 O. Tagit, D. Jańczewski, N. Tomczak, M. Y. Han, J. L. Herek and G. J. Vancso, *Eur. Polym. J.*, 2010, **46**, 1397–1403.
- 18 Y. Han, Y. Liu, H. Zhao, A. Vomiero and R. Li, *J. Mater. Chem. B*, 2021, **9**, 4111–4119.
- 19 P. Haro-González, L. Martínez-Maestro, I. R. Martín, J. García-Solé and D. Jaque, *Small*, 2012, **8**, 2652–2658.
- 20 C. Wang, H. Lin, Z. Xu, Y. Huang, M. G. Humphrey and C. Zhang, *ACS Appl. Mater. Interfaces*, 2016, **8**, 6621–6628.
- 21 G. Lisensky, R. McFarland-Porter, W. Paquin and K. Liu, *J. Chem. Educ.*, 2020, **97**, 806–812.
- 22 C. Ünlü, *Opt. Mater.*, 2019, **89**, 361–367.
- 23 S. M. Kestir, S. Şahin Keskin, Ö. Ergüder, N. Ük, Y. Türker, I. Nar, L. Trabzon and C. Ünlü, *Dalton Trans.*, 2023, **52**, 5704–5714.
- 24 M. Erkan, N. Ük, I. Nar and C. Ünlü, *Opt. Mater.*, 2023, **138**, 113713.
- 25 C. D. Dieleman, W. Ding, L. Wu, N. Thakur, I. Bepalov, B. Daiber, Y. Ekinici, S. Castellanos and B. Ehrler, *Nanoscale*, 2020, **12**, 11306–11316.
- 26 R. Bonetti and W. O. Parker, *JAOCs, J. Am. Oil Chem. Soc.*, 2019, **96**, 1181–1184.
- 27 Z. Li, A. L. K. Lui, K. H. Lam, L. Xi and Y. M. Lam, *Inorg. Chem.*, 2014, **53**, 10874–10880.
- 28 K. Yu, P. Ng, J. Ouyang, M. B. Zaman, A. Abulrob, T. N. Baral, D. Fatehi, Z. J. Jakubek, D. Kingston, X. Wu, X. Liu, C. Hebert, D. M. Leek and D. M. Whitfield, *ACS Appl. Mater. Interfaces*, 2013, **5**, 2870–2880.
- 29 S. Wang, J. Yu, P. Zhao, S. Guo and S. Han, *ACS Omega*, 2021, **6**, 7139–7146.
- 30 S. Shen, L. Zhao and L. Guo, *Int. J. Hydrogen Energy*, 2010, **35**, 10148–10154.
- 31 Z. Chen, D. Li, W. Zhang, C. Chen, W. Li, M. Sun, Y. He and X. Fu, *Inorg. Chem.*, 2008, **47**, 9766–9772.
- 32 O. Cavdar, M. Baluk, A. Malankowska, A. Žak, W. Lisowski, T. Klimczuk and A. Zaleska-Medynska, *J. Colloid Interface Sci.*, 2023, **640**, 578–587.
- 33 D. Mutavdžić, J. Xu, G. Thakur, R. Triulzi, S. Kasas, M. Jeremić, R. Leblanc and K. Radotić, *Analyst*, 2011, **136**, 2391–2396.
- 34 G. Yadav and M. Ahmaruzzaman, *Mater. Sci. Eng. B*, 2023, 292.
- 35 L. Li, A. Pandey, D. J. Werder, B. P. Khanal, J. M. Pietryga and V. I. Klimov, *J. Am. Chem. Soc.*, 2011, **133**, 1176–1179.
- 36 G. Morselli, M. Villa, A. Fermi, K. Critchley and P. Ceroni, *Nanoscale Horiz.*, 2021, **6**, 676–695.
- 37 P. Zhao, T. Huang and K. Huang, *J. Phys. Chem. C*, 2007, **111**, 12890–12897.
- 38 N. Gao, R. Zhang, B. Chen, J. Zhang, X. Zhang and A. L. Rogach, *Nano Res.*, 2021, **14**, 2321–2329.
- 39 N. M. Huang, *J. Nanomater.*, 2011, **2011**, 815709.
- 40 D. Cai, X. Yuan, D. Zhu, H. Zhou, H. Li and J. Zhao, *Mater. Res. Bull.*, 2017, **94**, 241–246.
- 41 B. Lesiak, L. Kövér, J. Tóth, J. Zemek, P. Jiricek, A. Kromka and N. Rangam, *Appl. Surf. Sci.*, 2018, **452**, 223–231.
- 42 J. Ibarra, J. Melendres, M. Almada, M. G. Burboa, P. Taboada, J. Juárez and M. A. Valdez, *Mater. Res. Express*, 2015, **2**, 095010.
- 43 C. Ünlü, G. Ü. Tosun, S. Sevim and S. Özçelik, *J. Mater. Chem. C*, 2013, **1**, 3026–3034.
- 44 Y. Coşkun, F. Y. Ünlü, T. Yılmaz, Y. Türker, A. Aydoğan, M. Kuş and C. Ünlü, *ACS Omega*, 2022, **7**, 18840–18851.
- 45 F. Y. Ünlü and A. Aydoğan, *ACS Appl. Polym. Mater.*, 2023, **5**, 7193–7200.

